Age-structured red blood cell susceptibility and the dynamics of malaria infections

Philip G. McQueen* and F. Ellis McKenzie

Center for Information Technology and Fogarty International Center, National Institutes of Health, Bethesda, MD 20892

Edited by Burton H. Singer, Princeton University, Princeton, NJ, and approved April 22, 2004 (received for review December 11, 2003)

Malaria parasites and immune responses in an infected human interact on a dynamic landscape, in which a population of replicating parasites depletes a population of replenishing red blood cells (RBCs). These underlying dynamics receive relatively little attention, but they offer unique insights into the processes that control most malaria infections. Here, we focus on the observation that three of the four malaria-parasite species that infect humans are restricted to particular age classes of RBC. We explicitly incorporate this observation in models of infection dynamics to distinguish common from species-specific pressures on host immune responses, and we find that age structuring has profound effects on the course of infection. For all four species conditions exist under which the parasites may persist at low densities, or may clear, even in the absence of an immune response. Catastrophic anemia can occur even with the two species that attack only the youngest RBCs, although only a small fraction of cells are parasitized at any point. Furthermore, with these two, compensatory erythropoetic responses in the host accelerate parasite population growth. A "basic reproduction rate" characterizes these differences in outcomes.

Malaria in a human begins with an inoculum of *Plasmodium* parasites from an *Anopheles* mosquito. The parasites penetrate liver cells, multiply, then enter the bloodstream, and invade red blood cells (RBCs), where they again multiply and burst the cells, each releasing 8–32 "merozoites" that invade more RBCs and continue the cycle. Almost all malaria pathology is associated with this blood stage replication cycle; it leads to geometric growth in the parasite population and to fevers, anemia, and sometimes death in the host (1).

Parasite population growth is usually constrained by host immune responses. Accordingly, most mathematical models of within-host dynamics have taken the general form of predator–prey models, with the predator a population of immune agents and the prey a population of *Plasmodium* (2). A few *Plasmodium falciparum* models attempt to relate the dynamics of the parasite population to those of its prey, the population of RBCs, but none incorporate RBC aging or age-structured susceptibility (3–7).

RBC age appears to be a strong constraint on malaria parasites, however: susceptibility to *Plasmodium vivax* or *Plasmodium ovale* invasion is said to be restricted to the very youngest circulating age class of RBCs, the "reticulocytes," and *Plasmodium malariae* invasion to the very oldest (8, 9). *P. falciparum*, the species responsible for almost all the 1–3 million deaths attributed to malaria each year, seems promiscuous with respect to its RBC targets (10). It is widely assumed that these age constraints explain why counts of parasitized RBCs rarely exceed 25,000 per μl with *P. vivax, P. ovale*, or *P. malariae*, but may reach 500,000 and beyond with *P. falciparum*, and thus, in turn, why fatal anemia occurs only in *P. falciparum* infections (11).

Most malaria infections are not fatal, but the mechanisms involved in their control are notoriously difficult to comprehend. Here, we use mathematical models to identify critical interactions between *Plasmodium* and RBC populations and indicate effects that immune responses must add (for instance, to counter the unexpectedly strong demands of *P. vivax* or *P. ovale*) if system dynamics are to resemble those observed in actual malaria infections.

The Models

RBCs emerge from bone marrow into the circulation, and in uninfected, healthy adults, they are removed by phagocytosis 120 days later (12). A density of ≈5 million RBCs per μl is maintained in adult males. The first 1–2 days of the RBC lifespan are the reticulocyte stage. Compensatory responses to anemia may boost RBC production to several times the basal level (12). We model the rate of RBC production as sensitive to changes in the rate of RBC destruction, with a response time of 48 h, and capped at some maximum given as a parameter value. Here we consider maximum RBC production fixed either at the basal rate [i.e., $(5 \times 10^6$ RBC per μl$)/(120$ days$) \approx 1{,}736$ RBC per μl per h] or at twice the basal rate.

Successful invasion of a RBC by a parasite depends on direct contact between the two. We take the contact process itself as random, with contact probabilities proportional to *Mer* and *V*, the densities of merozoites and uninfected susceptible RBCs, respectively. On contact, successful invasion depends on the receptor–ligand attachment(s) required for the physical process of invasion, which we model as a binding affinity ζ. Thus, infected RBCs are produced at rate $\zeta Mer V$. The details of RBC receptor usage by different *Plasmodium* species are not yet clear, in particular with respect to RBC age, but *P. vivax* invasion is limited to RBCs from Duffy-antigen-positive individuals, and *P. falciparum* can use multiple receptors (13); nothing is known about *P. malariae* receptors. Nothing is known about receptors for *P. ovale* except that they must differ from those for *P. vivax*; given their shared restriction to reticulocytes, however, we treat *P. ovale* as identical with *P. vivax* and refer only to the latter.

Therefore, we model age-structured attacks on RBCs as either (*i*) a *P. vivax*-like attack on reticulocytes or (*ii*) a *P. malariae*-like attack on senescent RBCs, and set the exact duration of RBC susceptibility in each model as a parameter value. For comparison, we model attacks on RBCs that present appropriate receptors at all ages: a fraction β of RBCs that emerge from marrow has life-long susceptibility; initially, at the start of infection, a fraction β of each RBC age cohort in circulation is susceptible. Hence, we call this attacker a generalist; it is believed $\beta \approx 1$ for *P. falciparum* (13).

Fig. 1 gives schematic representations of the models, which we formulated as compartmental differential equation systems (CODEs); CODEs allow us to include uncertainty in the duration τ of a process, such as RBC aging or parasite development in a RBC. Variance is set by $\tau/F^{1/2}$, where F is the number of compartments used to describe the process; variances are integral to models' steady-state solutions as well (see supporting information, which is published on the PNAS web site). Each model simulation mimicked 10^5 h of infection (≈11.4 yr), unless

This paper was submitted directly (Track II) to the PNAS office.

Abbreviations: CODE, compartmental differential equation system; ODE, ordinary differential equation.

*To whom correspondence should be addressed. E-mail: mcqueenp@helix.nih.gov.

POPULATION BIOLOGY

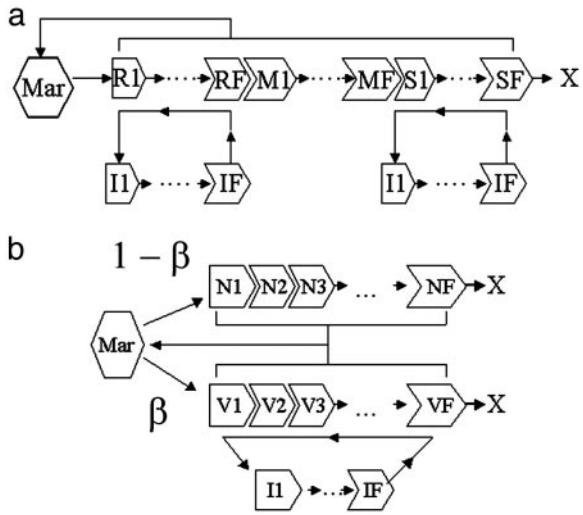

Fig. 1. Schematic of model dynamics. Bone marrow (Mar) is the source of new RBCs. (*a*) Age-structured models for *P. vivax* and *P. malariae* infections. RBC stages R1–RF are reticulocytes, susceptible to *P. vivax*, and S1–SF are senescent, susceptible to *P. malariae*; M1–MF are nonsusceptible stages. I1–IF are infected RBCs. (*b*) Generalist model. V1–VF are the vulnerable subset of RBCs, N1–NF are the nonvulnerable subset; β is the fraction of RBCs produced from marrow that are vulnerable. In all three models, RBC production is regulated by the rate of loss of RBCs by means of normal senescence or infection. Simulations mimic 10^5 h of infection unless the uninfected RBC count falls to <75% of its initial value (catastrophic anemia). X marks the natural end of the RBC lifespan.

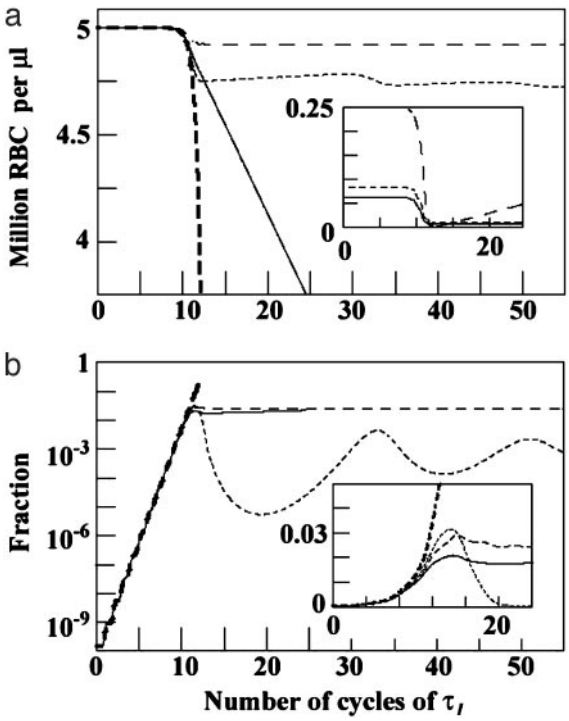

Fig. 2. Time course of infection. The time since primary release (horizontal axis) is shown as multiples of τ_I (3 days for *P. malariae* and 2 days for the others). In each case ζ is set so that $\mathbf{R_0} = 80/13$ (or ≈6.15). Lines are coded as: —, *P. vivax* with reticulocyte duration = 36 h; – –, *P. malariae* with senescent RBC duration = 48 h; - - -, generalist with $\beta = 0.05$; – – –, generalist with $\beta = 0.99$. (*a*) Uninfected RBC count. (*Inset*) The count of vulnerable RBCs for the *P. vivax*, *P. malariae*, and generalist $\beta = 0.05$ models. (*b*) The fraction of RBCs that are infected. (*Inset*) Enlargement of the region around 10 τ_I, showing the structure in the ''hump.'' Note the linear (instead of log) vertical scale of *Inset*.

the density of uninfected RBCs declined to 75% of its initial value, which we set as the threshold for catastrophic anemia, in which case the simulation halted. During the first simulated hour 10^4 merozoites were infused into a total blood volume of 5 liters to mimic primary release from the liver. We take the nominal time τ_I for a parasite to develop in a RBC as 72 h for *P. malariae* and 48 h for *P. vivax* and the generalist, and we use a compartment size of a half-hour. Then, the variance in τ_I is ≈6 h for *P. malariae* and ≈4.9 h for *P. vivax* and the generalist, in line with recent work (3).

When released from a bursting RBC, a free merozoite will die or be cleared from circulation within a time τ_{MER}, believed to be minutes (14). Thus, two competing Poisson processes affect the fate of merozoites: (*i*) they are removed from the blood at rate $1/\tau_{\mathrm{Mer}}$; (*ii*) they attach to RBCs at rate ζV. The probability that a merozoite infects a RBC rather than being cleared is $\zeta V \tau_{\mathrm{MER}} (1 + \zeta V \tau_{\mathrm{MER}})^{-1}$ (see supporting information). Thus, if $\tau_{\mathrm{MER}} \ll \tau_I$, its average number of descendants after a development cycle is

$$\mathbf{R} = p\zeta V \tau_{\mathrm{MER}} (1 + \zeta V \tau_{\mathrm{MER}})^{-1}, \qquad [1]$$

where p is the average number of merozoites released from a bursting RBC. We define $\mathbf{R_0}$, the basic reproduction rate, as the value of $\mathbf{R}$ at the beginning of the infection. This quantity both determines the initial behavior of an infection and affects its outcome. Nontrivial steady-state solutions exist only if $\mathbf{R_0} > 1$ (see supporting information). Thus, the parasite count ultimately vanishes if $\mathbf{R_0} < 1$, persists at its initial value if $\mathbf{R_0} = 1$, or converges to a larger steady state if $\mathbf{R_0} > 1$, unless the host RBC count is depleted to the point of catastrophic anemia. We stress that $\mathbf{R}$ (as opposed to $\mathbf{R_0}$) can change during the course of infection as V changes; in particular, $\mathbf{R} \to 1$ as a steady state is approached. Note that the existence of a noncatastrophic steady state does not preclude the possibility that catastrophic anemia will occur in the approach.

$T_{\mathrm{INF}} = 1/\zeta V = (p - \mathbf{R_0})\tau_{\mathrm{MER}}/\mathbf{R_0}$ gives the average time required for a merozoite to contact and invade a RBC. If $p = 16$ and $\tau_{\mathrm{MER}} = 0.1$ h, then $T_{\mathrm{INF}} = 1.35$ h, 2 min, or 0 if $\mathbf{R_0} = 1.1$, 12, or 16, respectively. Thus, despite our built-in assumption of free mixing, parasite transmission from RBC to RBC approaches a contact process as $\mathbf{R_0} \to p$. The generalist model is not an exact description of *P. falciparum* because *P. falciparum*-infected RBCs sequester and rosette with uninfected RBCs, which suggests that many merozoites travel minimal distances to invade RBCs (15). Nor do we consider invasions of a single RBC by multiple merozoites, a relatively rare event that is most frequent with *P. falciparum* (16). However, because $\mathbf{R_0}$ seems to be near p, at least in malaria-naive malaria-therapy patients (3), the behavior of the generalist model for $\beta \approx 1$ and large $\mathbf{R_0}$ may be fairly realistic for *P. falciparum*.

Here, we set $\tau_{\mathrm{Mer}} = 0.1$ h and $p = 16$. Calculations with other values of τ_{Mer} or p do not alter the qualitative conclusions here (see supporting information). Because merozoite counts directly reflect infected RBC counts, we report only the infected RBC counts.

Model Dynamics

In all three models, the value of $\mathbf{R_0}$ determines the infection dynamics until susceptible RBCs are significantly depleted. We would expect this to occur by time $T_C \approx \tau_I \log(V_o/\mathrm{Mer}_o)/\log \mathbf{R_0}$ (see supporting information). At this point the dynamics of the models diverge, as is evident in Fig. 2, which plots four time series: the *P. vivax* model with reticulocyte stage duration = 36 h, the *P. malariae* model with senescent RBC duration = 48 h, and the generalist model with $\beta = 0.05$ and $\beta = 0.99$. For

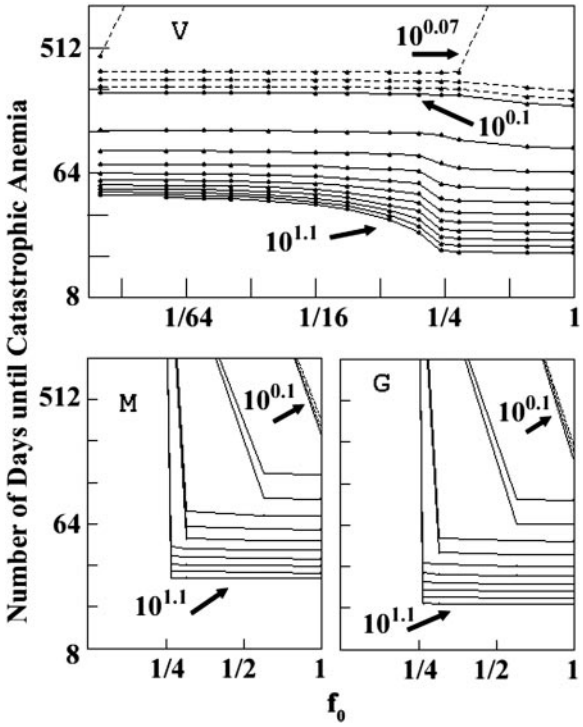

Fig. 3. Time to catastrophic anemia as a function of $\mathbf{f_0}$, the initial fraction of RBCs susceptible to infection. (*Upper*) *P. vivax*. (*Lower Left*) *P. malariae*. (*Lower Right*) Generalist. The solid curves are contours of $\mathbf{R_0}$ from $10^{0.1}$ to $10^{1.1}$, spaced so that log $\mathbf{R_0}$ changes by 0.1. The dotted lines are contours for $\mathbf{R_0} < 0.1$, spaced so that log $\mathbf{R_0}$ changes by 0.01.

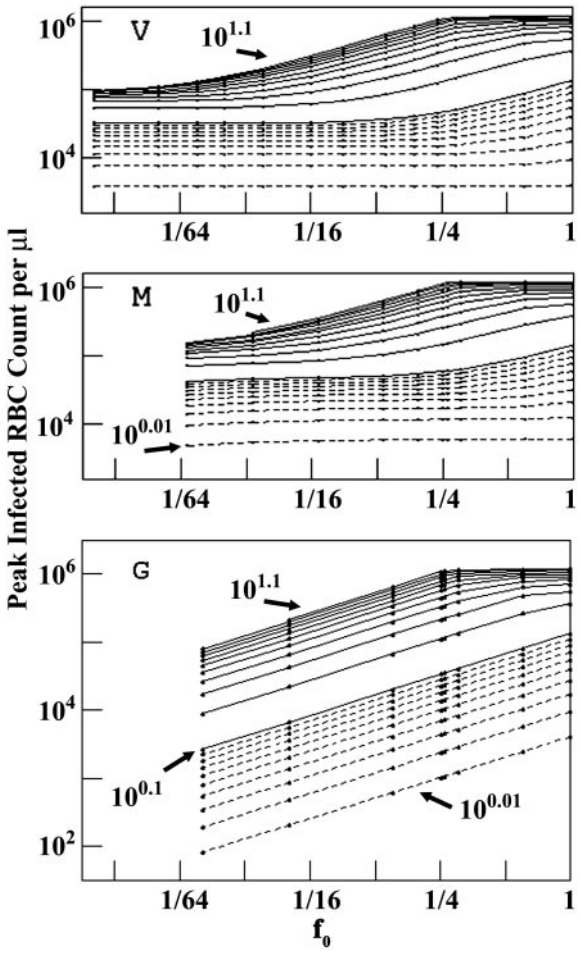

Fig. 4. Peak count of infected RBCs, $\mathbf{I_{PK}}$, as a function of $\mathbf{f_0}$. (*Top*) *P. vivax*. (*Middle*) *P. malariae*. (*Bottom*) Generalist. Contours are as in Fig. 3.

each model, RBC production was held at the basal rate and $\mathbf{R_0}$ set to 80/13 (≈6.15). Note that all four models are initially in lockstep, with parasite density growing exponentially for the first 9–12 cycles of τ_I (as expected from the T_C formula). After the first few weeks of the $\beta = 0.99$ generalist infection, the density of uninfected RBCs quickly collapses and the fraction of RBCs infected soars. For the $\beta = 0.05$ generalist and *P. malariae* infections, the density of uninfected RBCs is only mildly affected and the fraction of RBCs infected never exceeds ≈3%. The *P. vivax* infection leads to catastrophic anemia, however, although the maximum fraction of RBCs infected is ≈2%. The initial fraction of RBCs susceptible to *P. vivax* is only 36 h/120days = 0.0125, but *P. vivax* attack has more drastic clinical consequences than the $\beta = 0.05$ generalist, because targeted culling of reticulocytes ensures that few remain to mature and replenish the older RBCs.

Differences in model dynamics are also apparent in Fig. 3, which, for a range of $\mathbf{R_0}$ values >1, plots the time until the onset of catastrophic anemia as a function of $\mathbf{f_0}$, the fraction of RBCs initially susceptible (β for the generalist, and the susceptible-stage duration/120 days for the other two models; $\mathbf{f_0} = 0.0125$ and 0.0167, respectively, for the *P. vivax* 36-h and *P. malariae* 48-h examples in Fig. 2). In the generalist and *P. malariae* models, the density of uninfected RBCs declines to 75% of its initial value, our threshold for catastrophic anemia, only if $\mathbf{f_0} > 0.25$. In the *P. vivax* model, however, catastrophic anemia can occur even with $\mathbf{f_0} \approx 0.01$ and $\mathbf{R_0}$ barely >1. Even with a reticulocyte duration of just 18 h ($\mathbf{f_0} = 0.00625$) and $\mathbf{R_0} = 10^{0.06}$ (≈1.15), catastrophic anemia would occur in ≈450 days; the peak infected RBC count would be 2.1×10^4 per μl, so the fraction of RBCs infected would never exceed $(2.1 \times 10^4)/(3.75 \times 10^6 + 2.1 \times 10^4) \approx 0.6\%$. With a 36-h reticulocyte duration and $\mathbf{R_0} = 10$, the fraction of RBCs infected would never exceed ≈3%, but catastrophic anemia would occur within 45 days.

P. vivax model behaviors begin to resemble those of the other two models if the reticulocyte duration expands to encompass > ≈30% of the RBC lifespan; mature RBCs constitute a smaller fraction of the total RBC count, so choking off their predecessor reticulocytes has less effect. This is especially evident for $\mathbf{R_0}$ near 1, as can be seen in Fig. 3 and in the steady state (see supporting information).

Fig. 4 shows the peak infected RBC counts, $\mathbf{I_{PK}}$, corresponding to Fig. 3. Age-structured attacks produce striking differences: for a given $\mathbf{R_0}$ and $\mathbf{f_0}$, $\mathbf{I_{PK}}$ is higher in *P. vivax* and *P. malariae* models than in the generalist model. All RBCs emerging from bone marrow reach the stage susceptible to *P. vivax* or *P. malariae*, whatever the value of $\mathbf{f_0}$, either immediately (*P. vivax*) or after aging (*P. malariae*). For the generalist, however, only a fraction β of new RBCs enters the susceptible pool. $\mathbf{I_{PK}}$ curves for the generalist approach those of the other two models as $\mathbf{f_0} \to 1$. Age-structured attacks also differ in their steady-state values (see supporting information).

For $\mathbf{R_0} < 1$, all three models effectively have the same stiff but analytically solvable ordinary differential equation (ODE) system. As $\mathbf{R_0} \to 1$, to a very good approximation the time required for the initial parasite population to decrease by $1/e$ (the e-folding time) is $-\tau_I/\ln \mathbf{R_0}$. If $\tau_I = 48$ h, the e-folding time is ≈19 days for $\mathbf{R_0} = 0.9$ and ≈199 days for $\mathbf{R_0} = 0.99$. Thus nonsustainable infections with $\mathbf{R_0}$ just below the threshold of persis-

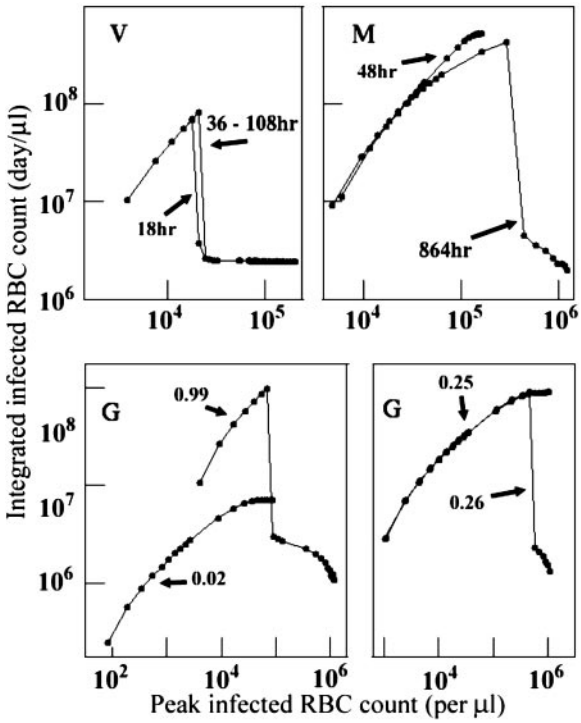

Fig. 5. Integrated parasite count, I_{INT}, vs. peak parasite count, I_{PK}, for representative values of susceptible-stage duration (*P. vivax* in *Upper Left* and *P. malariae* in *Upper Right*) or β (generalist in the two *Lower* sections). On each curve, the points correspond to values of $\mathbf{R_0}$ used in Figs. 3 and 4, from $10^{0.01}$ on the left to $10^{1.1}$ on the right.

tence could linger, at undetectable densities, with the host vulnerable to increases in p or ζ.

Integrated Parasite Count

As a proxy for the cumulative number of parasites produced in an infection, we define the integrated infected RBC count $\mathbf{I_{INT}}$ = (average infected RBC count) × (duration of simulated infection). Fig. 5 plots $\mathbf{I_{INT}}$ vs. $\mathbf{I_{PK}}$ for key values of $\mathbf{f_0}$. $\mathbf{R_0}$ varies from $10^{0.01}$ to $10^{1.1}$ along each curve, tracking $\mathbf{I_{PK}}$. The maximum $\mathbf{I_{INT}}$ for each model occurs at a distinct combination of $\mathbf{R_0}$ and $\mathbf{f_0}$ values, e.g., a relatively small $\mathbf{R_0}$ (1.17) and large $\mathbf{f_0}$ (0.99) for the generalist, large $\mathbf{R_0}$ (>12) and intermediate $\mathbf{f_0}$ (0.25) for *P. malariae*. With small $\mathbf{f_0}$ values in the generalist or *P. malariae* models, $\mathbf{I_{INT}}$ is monotonic in $\mathbf{I_{PK}}$, but large $\mathbf{f_0}$ values lead to catastrophic anemia: $\mathbf{I_{INT}}$ abruptly collapses with increased $\mathbf{I_{PK}}$ as $\mathbf{f_0}$ exceeds 0.25. Again, the *P. vivax* model differs dramatically: the $\mathbf{I_{INT}}$ vs. $\mathbf{I_{PK}}$ curve is relatively insensitive to reticulocyte duration, and the largest values of $\mathbf{I_{INT}}$ occur with $\mathbf{I_{PK}} < 30{,}000$ per μl, an order of magnitude lower than with the *P. malariae* or generalist models.

Compensatory Responses to Anemia

The preceding results assume that RBC production remains fixed at the basal rate throughout a malaria infection; in fact, significant RBC loss usually stimulates enhanced or accelerated production. The particular mechanisms involved are still poorly understood (17), but one recent analysis reported an average 37% increase in RBC production in adult first-time *P. falciparum* patients (18). Here, we allow RBC production to match RBC depletion, up to a maximum of twice the basal rate (Eq. **5**). Fig. 6 shows the effects of compensatory responses, with varying $\mathbf{R_0}$, in four model situations: *P. vivax* with 36-h reticulocyte duration, *P. malariae* with 48-h senescent RBC duration, and the generalist with $\beta = 0.05$ or 0.99.

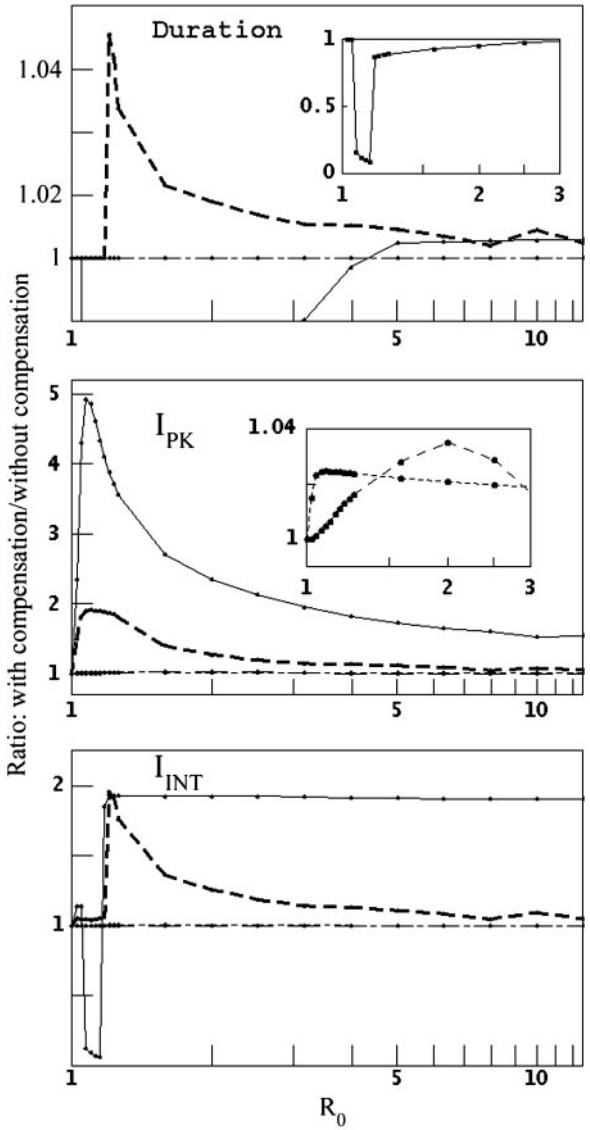

Fig. 6. Changes in dynamics when RBC production increases with RBC depletion. This figure compares the ratios of model results with compensation (i.e., the RBC production rate matches the RBC depletion rate, up to twice the basal rate) to those without compensation (basal rate only). Lines are coded as in Fig. 2. (*Top*, Duration) Time to catastrophic anemia. (*Middle*, I_{PK}) Peak count of infected RBCs. (*Bottom*, I_{INT}) Integrated parasite count. (*Upper Inset*) Demonstration that compensation substantially accelerates the onset of catastrophic anemia in *P. vivax* infection with $\mathbf{R_0} < 2$. (*Middle Inset*) Demonstration that compensation has relatively little effect on peak density in *P. malariae* or $\beta = 0.05$ generalist infections.

In the *P. vivax* model, the host gains little or no benefit from compensatory response. For $\mathbf{R_0} < 10^{0.6}$ (≈4), increased RBC production actually speeds the onset of catastrophic anemia. In contrast, compensation slightly delays the onset in the $\beta = 0.99$ generalist model. Compensation boosts peak parasite counts in all models, but most dramatically in the *P. vivax* model for $\mathbf{R_0} < 10^{0.4}$ (≈2.5). Consider the *P. vivax* model with $\mathbf{R_0} = 10^{0.05} \approx 1.122$, for instance: doubling the rate of RBC production quickly doubles the reticulocyte count, the *instantaneous* reproduction rate $\mathbf{R}$ becomes nearly twice $\mathbf{R_0}$ (2.097; Eq. **1**), and a nonlethal *P. vivax* infection becomes lethal. Compensation also boosts the integrated count, with the notable exception of *P. vivax* with $\mathbf{R_0}$

$< 10^{0.1}$ ($\approx$1.25), the regime in which nonlethal infections turn lethal. If infection *reduces* RBC production rates, the onset of catastrophic anemia with *P. vivax* is delayed, and $\mathbf{I_{PK}}$ decreases, consistent with a reduction of **R** (see supporting information).

Discussion

Our results show that age-restricted RBC susceptibility strongly influences the dynamics of *Plasmodium* infection and thus the imperatives for host immune response. They conform to clinical observations: if we limit susceptibility to the small fraction of RBCs that are senescent, infections are relatively benign, as is *P. malariae*. They suggest that compensatory RBC production usually aggravates infections; in fact, it may be functionally suppressed in chronically exposed patients (17). However, our results argue against the belief that, because only a small fraction of RBCs are reticulocytes, *P. vivax* and *P. ovale* are intrinsically less dangerous than *P. falciparum*: attacks on reticulocytes choke off the supply of mature RBCs and lead to catastrophic anemia; control demands aggressive reactions.

Insights into RBC dynamics should aid in assessing interventions, most obviously exchange transfusion (19), but also drugs or potential vaccines. With age-restricted susceptibility, uninfected RBCs can graduate into or out of a susceptible class, but depletion of that class depletes older ones. Future work must identify more precise age-associated RBC characteristics that govern susceptibility, however. Because circulating RBCs are anucleate and cannot synthesize new surface molecules, receptors that decay cannot be replaced; reticulocyte susceptibility to *P. vivax* may be related to higher Duffy-antigen density, for instance (20). If RBC susceptibility to *P. malariae* is related to senescence markers, the accelerated senescence of uninfected RBCs reported with *P. falciparum* (21) should greatly affect mixed-species infections (22). The common portrayal of *P. falciparum* as a generalist is complicated by evidence of a seeming preference for young RBCs (23), but more detailed resolution is needed here as well: our model shows that the proportion of RBCs that is in young age classes increases as an infection proceeds.

Similarities and differences in immune response to different *Plasmodium* species remain obscure partly due to preoccupation with *P. falciparum*. Duffy, sickle-cell and other RBC polymorphisms indicate that malaria has shaped human immunity in more than the usual, proximate sense of the term, however. The four species that infect humans diverged long ago, their histories with non-human hosts differ, and comparing their traits should be informative (24). For instance, in humans, *P. vivax* induces fever at much lower densities than *P. falciparum* (25), which suggests accelerated activation of innate responses; the relatively slow growth of *P. malariae* may allow more reliance on the agents of acquired responses (26).

Our results show that, in the absence of immune responses, direct parasite-induced hemolysis can cause anemia. In some malaria patients a "bystander" effect may contribute to anemia: increased macrophage activity removes uninfected and infected RBCs, destroying perhaps 8.5 uninfected RBCs for each bursting infected RBC (18). Diserythropoesis may also contribute to anemia (17). Although we do not explore any effects of immune responses here, we crudely mimicked these effects in simulations, and, as expected, the usual result was accelerated onset of catastrophic anemia (see supporting information). However, it should be clear that in their current form our models cannot resolve the debate about which factor is the major cause of sustained anemia in actual *P. falciparum* infections (3, 18). Our results show that age-structured RBC susceptibility is an important, previously unappreciated determinant of malaria infection dynamics, to be considered in future work.

We do not consider parasite synchronization, which is likely immune-mediated (27), but note that it would probably benefit the host of a *P. vivax* infection were reticulocyte susceptibility <48 h. We also do not consider the blood stages transmissible to mosquitoes; their production entails complex trade-offs between density, persistence, pathogenesis, and transmission (28, 29), but these should not alter the qualitative conclusions given here. Here, any correlates of the peak infected RBC count would be maximized simply by maximizing $\mathbf{R_0}$ and $\mathbf{f_0}$; larger $\mathbf{R_0}$ values also lead more quickly to catastrophic anemia, however, and correlates of the integrated infected RBC count would be maximized by species-specific balances between $\mathbf{R_0}$ and $\mathbf{f_0}$. Finally, although our results are scaled on a per-microliter basis, we note that any given number of parasites represents a higher proportion of the RBC total in a child than in an adult, which may add to response imperatives.

Mathematical Formalism

We model the infection dynamics with systems of CODEs. The notation is as in Fig. 1. The CODEs for the infected RBCs are:

$$\begin{aligned} dI_1/dt &= \zeta\, Mer(t)V - \kappa_I I_1 \\ dI_n/dt &= \kappa_I(I_{n-1} - I_n), \quad 1 < n \le \mathrm{FI} \end{aligned} \qquad [2]$$

where FI is the number of compartments and $\kappa_I = \mathrm{FI}/\tau_I$. Given its short duration, we use a single ODE for the merozoite:

$$dMer/dt = p\kappa_I I_{\mathrm{FI}} - \zeta\, Mer(t)V - Mer/\tau_{Mer} + L(t). \qquad [3]$$

V is the total count of vulnerable RBCs. $L(t)$ describes the primary infusion of merozoites from the liver into the blood, the details of which are unknown beyond that it occurs quickly ($\approx$1 h), with just 10^4-10^5 parasites released (1). We took a tent form for $L(t)$, which allows for some control in the time profile of release:

$$\begin{aligned} L(t) &= b^* t \text{ for } 0 < t < t_{\mathrm{MX}} \\ &= c - d^*(t - t_{\mathrm{MX}}) \text{ for } t_{\mathrm{MX}} < t < t_{\mathrm{MX}} + t_D \\ &= 0 \text{ otherwise.} \end{aligned} \qquad [4]$$

The release is at its maximum rate at $t = t_{\mathrm{MX}}$ and concludes at $t = t_D$. Parameters b, c, and d are fixed uniquely for a given t_{MX} and t_D by requiring $L(t)$ to be continuous with time integral equal to $10^4/(5 \times 10^6$ mm). Details of $L(t)$ had little effect on model dynamics, because the number released is small and t_D is no more than a few hours (results not shown). For simulations reported here, $t_{\mathrm{MX}} = 0.5$ h and $t_D = 1$ h.

The RBC source has its own ODE:

$$\begin{aligned} ds(t)/dt &= \lambda_{\mathrm{So}}(s_0 - U_{\mathrm{T}} - s(t)), s_0 - U_{\mathrm{T}'} < s_{\mathrm{MX}} \\ &= \lambda_{\mathrm{So}}(s_{\mathrm{MX}} - s(t)), s_0 - U_{\mathrm{T}'} > s_{\mathrm{MX}}. \end{aligned} \qquad [5]$$

λ_{So} is the rate of response of the source to changes in the RBC count. We took $1/\lambda_{\mathrm{So}} = 2$ days (12). U_{T} is the time rate of change in the total count of uninfected RBCs, s_0 is the normal rate of new RBC production, and s_{MX} is the maximum rate.

The CODEs for the susceptible (R) and nonsusceptible (M) RBCs in the *P. vivax* model are:

$$\begin{aligned} dR_1/dt &= s(t) - \kappa_R R_1 - \zeta Mer(t) R_1 \\ dR_n/dt &= \kappa_R(R_{n-1} - R_n) - \zeta Mer(t) R_n,\ 1 < n \le \mathrm{FR} \\ dM_1/dt &= \kappa_R\, R_{\mathrm{FR}} - \kappa_M M_1 \\ dM_n/dt &= \kappa_M(M_{n-1} - M_n),\ 1 < n \le \mathrm{FM}, \end{aligned} \qquad [6]$$

where $\kappa_R = \mathrm{FR}/\tau_R$, and τ_R is the average reticulocyte duration. Based on what is known about RBC development (12), we took FR = 21 so that the variance in the reticulocyte stage duration is $\approx 0.22\tau_R$ (or ≈ 8 h if $\tau_R = 36$ h). $\kappa_M = \mathrm{FM}/\tau_M$, and τ_M is the nominal duration of the nonvulnerable stage (120 days $- \tau_R$). We choose FM so that $1/\kappa_M = 18$ h. The total count of the susceptible cells is $V = \sum_{n\,=\,1,\,\mathrm{FR}} R_n$.

The CODEs in the *P. malariae* model are:

$$\begin{aligned}
\mathrm{d}M_1/\mathrm{d}t &= s(t) - \kappa_E M_1\\
\mathrm{d}M_n/\mathrm{d}t &= \kappa_E(M_{n-1} - M_n),\ 1 < n \le \mathrm{FM}\\
\mathrm{d}S_1/\mathrm{d}t &= \kappa_E(M_1 - S_1) - \zeta\, Mer(t) S_1\\
\mathrm{d}S_n/\mathrm{d}t &= \kappa_E(S_{n-1} - S_n) - \zeta\, Mer(t) S_n,\ 1 < n \le \mathrm{FS}. \qquad \textbf{[7]}
\end{aligned}$$

FM/κ_E is the nominal duration of the nonvulnerable RBC stage, and FS/κ_E is the nominal duration of the senescent stage. We chose FM + FS so that $1/\kappa_E = 12$ h, for a RBC lifespan of 120 days. Here $V = \sum_{n\,=\,1,\,\mathrm{FR}} S_n$.

The CODEs in the generalist model are:

$$\begin{aligned}
\mathrm{d}V_1/\mathrm{d}t &= \beta s(t) - \kappa_E V_1\\
\mathrm{d}V_n/\mathrm{d}t &= \kappa_E(V_{n-1} - V_n) - \zeta\, Mer(t) V_n,\ 1 < n \le \mathrm{FE}\\
\mathrm{d}N_n/\mathrm{d}t &= (1 - \beta) s(t) - \kappa_E N_1\\
\mathrm{d}N_n/\mathrm{d}t &= \kappa_E(N_{n-1} - N_n),\ 1 < n \le \mathrm{FE}. \qquad \textbf{[8]}
\end{aligned}$$

We took $1/\kappa_E = 12$ h for both nonsusceptible and susceptible cells, and $V = \sum_{n\,=\,1,\,\mathrm{FR}} V_n$.

If at any point the merozoite count or the infected, susceptible or nonsusceptible RBC total drop to <1 for the whole volume of blood (here 5×10^6 μl), all the compartments that contribute to that particular total are reset to zero. All ODE systems were solved by using the fifth-order Runge–Kutta–Fehlberg algorithm, which incorporates an embedded fourth-order Runge–Kutta algorithm for adaptive stepsize control of the time integration (30, 31).

We thank David L. Smith, Barbara C. Sorkin, and an anonymous reviewer for critical comments.

1. White, N. J. & Breman, J. G. (2001) in *Harrison's Principles of Internal Medicine*, eds. Braunwald, E., Fauci, A. S., Isselbacher, K. J., Kasper, D. L., Hauser, S. L., Longo, D. L. & Jameson, J. L. (McGraw–Hill, New York) pp. 1203–1213.
2. Molineaux, L. & Dietz, K. (1999) *Parassitologia* **41,** 221–231.
3. Gravenor, M. B., McLean, A. R. & Kwiatkowski, D. (1995) *Parasitology* **110,** 115–122.
4. Hetzel, C. & Anderson, R. M. (1996) *Parasitology* **113,** 25–38.
5. Hoshen, M. B., Heinrich, R., Stein, W. D. & Ginsburg, H. (2000) *Parasitology* **121,** 227–235.
6. Gravenor, M. B., Lloyd, A. L., Kremsner, P. G., Missinou, M. A., English, M., Marsh, K. & Kwiatkowski, D. (2002) *J. Theor. Biol.* **217,** 137–148.
7. Haydon, D. T., Matthews, L., Timms, R. & Colegrave, N. (2003) *Proc. R. Soc. London Ser. B* **270,** 289–298.
8. McKenzie, F. E., Jeffery, G. M. & Collins, W. E. (2001) *J. Parasitol.* **87,** 626–637.
9. McKenzie, F. E., Jeffery, G. M. & Collins, W. E. (2002) *J. Parasitol.* **88,** 521–535.
10. Gilles, H. M. (1993) in *Bruce-Chwatt's Essential Malariology*, eds. Gilles, H. M. & Warrell, D. A. (Edward Arnold, London), pp. 12–34.
11. Krogstad, D. J. (1995) in *Principles and Practice of Infectious Diseases*, eds. Mandell, G. L., Bennett, J. E. & Dolin, R. (Churchill Livingstone, New York), pp. 2415–2427.
12. Rapaport, S. I. (1987) *Introduction to Hematology* (Lippincott, Philadelphia).
13. Miller, L. H., Baruch, D. I., Marsh, K. & Doumbo, O. K. (2002) *Nature* **415,** 673–679.
14. Johnson, J. G., Epstein, N., Shiroishi, T. & Miller, L. H. (1980) *Parasitology* **80,** 539–550.
15. Davis, T. M. E., Krishna, S., Looareesuwan, S., Supanaranond, W., Pukrittayakamee, S., Attatamsoonthom, K. & White, N. J. (1990) *J. Clin. Invest.* **86,** 793–800.
16. Simpson, J. A., Silamut, K., Chotivanich, K., Pukrittayakamee, S. & White, N. J. (1999) *Trans. R. Soc. Trop. Med. Hyg.* **93,** 165–168.
17. Wickramasinghe, S. N. & Abdalla, S. H. (2000) *Baillieres Best Pract. Res. Clin. Haematol.* **13,** 277–299.
18. Jakeman, G. N., Saul, A., Hogarth, W. L. & Collins, W. E. (1999) *Parasitology* **119,** 127–133.
19. Wilkinson, R. J., Brown, J. L., Pasvol, G., Chiodini, P. L. & Davidson, R. N. (1994) *Q. J. Med.* **87,** 553–557.
20. Woolley, I. J., Hotmire, K. A., Sramkoski, R. M., Zimmerman, P. A. & Kazura, J. W. (2000) *Transfusion* **40,** 949–953.
21. Omodeo-Sale, M. F., Motti, A., Basilico, N., Parapini, S., Olliaro, P. & Taramelli, D. (2003) *Blood* **102,** 705–711.
22. McKenzie, F. E. & Bossert, W. H. (1997) *J. Parasitol.* **83,** 593–600.
23. Pasvol, G., Weatherall, D. J. & Wilson, R. J. M. (1980) *Br. J. Haematol.* **45,** 285–295.
24. Paul, R. E. L., Ariey, F. & Robert, V. (2003) *Ecol. Lett.* **6,** 866–880.
25. Kitchen, S. F. (1949) in *Malariology*, ed. Boyd, M. F. (Saunders, Philadelphia) pp. 1027–1045.
26. Mason, D. P. & McKenzie, F. E. (1999) *Am. J. Trop. Med. Hyg.* **61,** 367–374.
27. Rouzine, I. M. & McKenzie, F. E. (2003) *Proc. Natl. Acad. Sci. USA* **100,** 3473–3478.
28. McKenzie, F. E. & Bossert, W. H. (1998) *J. Theor. Biol.* **193,** 419–428.
29. McKenzie, F. E. & Bossert, W. H. (1998) *Am. J. Trop. Med. Hyg.* **58,** 763–767.
30. Cash, J. R. & Karp, A. H. (1990) *ACM Trans. Math. Soft* **16,** 201–222.
31. Press, W. H., Teukolskky, S. A., Vettering, W. T. & Flannery, B. P. (1992) *Numerical Recipes in C* (Cambridge Univ. Press, Cambridge, U.K.).